

Manuscript accepted by *Geology*. The final publication is available via  
<https://pubs.geoscienceworld.org/gsa/geology/article-abstract/47/2/123/567988/widespread-seismic-anisotropy-in-earth-s-lowermost?redirectedFrom=fulltext>

1 Widespread seismic anisotropy in Earth's lowermost  
2 mantle beneath the Atlantic and Siberia

3 **Michael Grund and Joachim R. R. Ritter**

4 *Geophysical Institute, Karlsruhe Institute of Technology (KIT), Hertzstr. 16, 76187*  
5 *Karlsruhe, Germany*

6  
7 **ABSTRACT**

8       Deep inside the Earth, just above the core-mantle boundary at around 2,700 km  
9 depth, large-scale mantle structures are assumed to play a key role for global geodynamic  
10 processes. While unusual hot regions are attributed to feed rising mantle plumes and  
11 volcanic hotspots, the accumulation of subducted lithospheric plates is associated with  
12 colder than average features. In both environments the appearance of dynamic-driven  
13 processes such as deformation and mantle flow can directly be inferred by the presence of  
14 seismic anisotropy. However, the geometries as well as the interactions of these massive  
15 anomalous structures with the surrounding mantle material are still under debate. Based  
16 on new seismic data from a dense and large-aperture recording network in Scandinavia  
17 we characterize the anisotropic signatures of two so far unexplored regions in the  
18 lowermost mantle by using observations of clearly discrepant SKS-SKKS shear wave  
19 splitting measurements. Thereby we can demonstrate that anisotropy is located along the

20 northern edges of the Large Low Shear Velocity Province beneath Africa. Furthermore,  
21 we recover an anisotropic structure in a region of fast seismic velocity underneath Siberia  
22 which provides additional evidence for widespread deformation caused by a deeply  
23 subducted slab.

## 24 **INTRODUCTION**

25 Teleseismic core-refracted shear waves such as SKS and SKKS sample nearly the  
26 same volumes in the upper 500 km of the Earth's mantle for the same source-receiver  
27 pair. In contrast, their raypaths differ significantly in the lower mantle (Fig. 1). With the  
28 exception of the 200–300 km-thick D'' layer just atop the core-mantle boundary (CMB)  
29 the lower mantle is generally assumed to be nearly isotropic (e.g., Meade et al., 1995).  
30 Therefore, distinct discrepancies in SKS-SKKS shear wave splitting are a powerful tool  
31 to map depth-dependent anisotropic anomalies in D'' (e.g., Lynner and Long, 2014).  
32 Recently the observations of discrepant SKS-SKKS splitting pairs increased, especially  
33 for areas along the edges of the Large Low Shear Velocity Provinces (LLSVPs) beneath  
34 Africa and the Pacific (e.g., Niu and Perez, 2004; Lynner and Long, 2014; Deng et al.,  
35 2017) or for more meso-scale structures like the Perm Anomaly beneath Russia (Long  
36 and Lynner, 2015). It was inferred that variations of complex and strong anisotropy are  
37 located near the boundaries of LLSVPs which are potentially associated with deformation  
38 due to mantle flow (e.g., Cottaar and Romanowicz, 2013). Furthermore, there is evidence  
39 from SKS-SKKS splitting for anisotropy in D'' caused by remnants of paleo-subducted  
40 slab material that induces high shear deformation atop the CMB (e.g., Long, 2009).

41 Here we present striking new observations of discrepant SKS-SKKS splitting  
42 pairs that were recorded across a large-aperture seismic network in Scandinavia and

43 surrounding countries. With our findings we can shed light on two widespread and so far  
44 poorly sampled or fully unexplored anomalous regions in D'' that are located along the  
45 northern edges of the African LLSVP and beneath northwestern Siberia in an area of  
46 consistent fast seismic shear wave velocity ( $v_S$ ). The knowledge on such anomalies  
47 provides rare constraints for improved modeling and understanding of mantle dynamics.

## 48 **DATA AND METHODS**

49 We analyzed seismic data of more than 250 temporary and permanent stations  
50 (Fig. 1) that are mainly part of the ScanArray network (Thybo et al., 2012; Grund et al.,  
51 2017). Earthquakes with  $M_W > 5.8$  at distances of  $80^\circ$ - $140^\circ$  were selected for the routine  
52 shear wave splitting analysis. Here we only focus on a subset of the whole analyzed data  
53 set, namely events for which it was possible to identify both clear SKS and SKKS  
54 arrivals on the same seismogram (Table DR1 in the GSA Data Repository<sup>1</sup>). Shear wave  
55 splitting (fast axis  $\phi$  and delay time  $\delta t$ ) was measured with the SplitLab package  
56 (Wüstefeld et al., 2008), using simultaneously the rotation correlation method (RC,  
57 Bowman and Ando, 1987) and the energy minimization method (SC, Silver and Chan,  
58 1991). Prior to the measurements we checked the sensor orientations (see Data  
59 Repository for details) and processed the waveforms using a zero-phase bandpass filter  
60 (5–15 s). For some recordings the corner periods were slightly adjusted to improve the  
61 signal-to-noise ratio (SNR) as done in previous studies (e.g., Long, 2009; Grund, 2017).  
62 We only consider measurements that agreed for both methods (RC and SC) within their  
63 error bounds (95% confidence region) and which have an  $\text{SNR} \geq 5$ . All splitting  
64 measurements (Table DR1) have typical errors of less than  $\pm 25^\circ$  for  $\phi$  (average:  $\pm 15.5^\circ$ )  
65 and  $\pm 0.5$  s for  $\delta t$  ( $\pm 0.32$  s). For error estimation we applied the corrected equations by

66 Walsh et al. (2013) as implemented in the StackSplit plugin (Grund, 2017). Phase arrivals  
67 with a clear signal on the radial component,  $\text{SNR} \geq 5$  and (nearly) linear particle motion  
68 before the correction for splitting were classified as so-called nulls (no splitting). In our  
69 data set we classified a pair of SKS-SKKS as discrepant if one phase was null and the  
70 other phase was clearly split. If both phases were split (similar  $\phi$  and  $\delta t$ ) or both were  
71 null, the pair was considered as non-discrepant (e.g., Long and Lynner, 2015). In order to  
72 characterize contributions from lowermost mantle (LMM) anisotropy at stations with  
73 complex splitting characteristics (Fig. DR2), we followed the approach of Deng et al.  
74 (2017) by measuring the splitting intensity (SI) as described by Chevrot (2000). Based on  
75 this approach null arrivals in our data set have to fulfill the condition of an absolute SI  
76 value that is  $< 0.2$  and for a discrepant SKS-SKKS pair the absolute SI-difference ( $\Delta\text{SI}$ )  
77 including the errors has to be  $\geq 0.2$ . For a potential contribution from LMM-anisotropy,  
78  $\Delta\text{SI}$  between SKS and SKKS is expected to be at least  $\geq 0.4$  (Deng et al., 2017).

## 79 **RESULTS AND DISCUSSION**

### 80 **Observation of Clearly Discrepant SKS-SKKS Waveforms**

81 Using shear wave splitting analysis, in total we received 332 pronounced SKS-  
82 SKKS pairs. (Table DR1). Out of these, 49 pairs show clear discrepancies and 283 pairs  
83 offer no anomalous pattern. Figure 2 presents a waveform example of a discrepant SKS-  
84 SKKS pair. Further recordings are shown in Figure DR3. If possible we cross-checked  
85 the SKS results by measuring splitting also for sSKS. Both phases sample nearly the  
86 same volumes along their raypaths and, as expected, the splitting parameters reveal  
87 consistency within the limits of uncertainty (Fig. DR4).

88 Taking into account finite frequency effects (e.g., Favier and Chevrot, 2003), it is  
89 quite unlikely that such waveform discrepancies originate only from shallow anisotropy  
90 directly beneath the station. With dominant periods of 6–10 s, the Fresnel zones for SKS  
91 and SKKS overlap significantly in the mantle transition zone and uppermost lower  
92 mantle (Fig. DR5). For this reason both phases of a pair are sensitive to the same volume  
93 and we would expect the same  $\phi$ - $\delta t$  characteristics. Furthermore, we rule out major  
94 influences due to waveform interference between phases arriving at the stations within  
95 short time periods (Lin et al., 2014). The observed discrepancies occur for distances of  
96  $100^\circ$ - $130^\circ$  and event depths  $> 20$  km (Fig. DR6). This was assumed to be sufficient to  
97 avoid dominant interference effects (Deng et al., 2017) (Figs. DR7, DR8). Hence, our  
98 observed SKS-SKKS discrepancies are first-order indicators that a component of LMM-  
99 anisotropy plays a key role in this context. However, for observations of non-discrepant  
100 pairs (Fig. DR4) a contribution of LMM-anisotropy cannot necessarily be ruled out (e.g.,  
101 Long and Lynner, 2015). Depending on the raypaths and the dimension of an anomaly  
102 with consistent anisotropic properties ( $\phi$ ,  $\delta t$ ), both phases could be equally split or not  
103 split (Fig. DR9).

104 In order to detect any geographical correlation between the splitting discrepancies  
105 and large-scale LMM features, we summarize our results in Figure 3 along with the  
106 GyPSuM global vs tomography model (Simmons et al., 2010) and the pierce points of the  
107 SKS-SKKS raypaths in 2,700 km depth. Due to contributions from shallower anisotropy  
108 in the upper mantle, at most stations in our network the splitting pattern is not well-  
109 constrained or it indicates a non-simple nature of anisotropy (Fig. DR2). Thus, we  
110 explicitly cannot correct for likely upper mantle contributions here as done in previous

111 studies with more simple splitting characteristics (e.g., Lynner and Long, 2014).  
112 Nevertheless, the evaluation of measured  $\Delta SI$  allows to explore potential contributions of  
113 LMM-anisotropy to the overall splitting signals (Deng et al., 2017).

#### 114 **Geographic Clusters in the Lowermost Mantle**

115 From the locations of the D'' pierce points, the anomalous pairs can be divided  
116 into a western and eastern region relative to our station network (Fig. 3). As observed in  
117 previous SKS-SKKS studies, the pierce points of discrepant pairs are interleaved by non-  
118 discrepant ones that are mostly null/null observations (especially for phase arrivals from  
119 west). A possible explanation is that small-scale heterogeneity of anisotropic structure is  
120 located along the slightly varying raypaths in the LMM (e.g., Long and Lynner, 2015).

121 For the eastern region we observe two types of discrepant splitting pairs. First, a  
122 set of 22 pairs with split SKKS phases and clear nulls for SKS. The split SKKS phases  
123 sample the LMM roughly along an east-west transect (65°N, 60°-92°E) near the edges of  
124 a major fast- $v_S$  anomaly in D'' beneath northwestern Siberia (Fig. 3). Besides nearly  
125 consistent orientations for  $\phi$  (average 5.3°),  $\Delta SI$  is  $> 0.4$  for the majority of pairs (Fig.  
126 DR10). Moreover, these pairs were recorded at stations that are located on different  
127 geological units from southwest Sweden up to northern Finland (Figs. DR7-DR8, DR11).  
128 Therefore, such a consistent splitting pattern indicates a large-scale feature of uniform  
129 LMM-anisotropy beneath northwestern Siberia that is observed independently from  
130 structures directly underneath the network. In contrast, the second group in the east  
131 consists of six pairs with split SKS and nulls for SKKS. Beyond that, the orientations for  
132  $\phi$  with nearly east-west alignments differ significantly compared to the first group. The  
133 SKS pierce points in D'' are located within a narrow north-south swath (60°-72°N, 45°E)

134 that encompasses areas with strong variations in  $v_s$ . The two split SKS phases in the  
135 south fall into a region of anomalously low  $v_s$  that is known as Perm Anomaly (Fig. 3).

136 Within the western cluster most pierce points of the split SKKS phases cover a  
137 nearly north-south oriented area in the LMM beneath the Atlantic west of UK and  
138 northwest of France. For the orientations of  $\phi$  (only split SKKS) we also determined  
139 consistent directions (average of  $39^\circ$ ) whereas  $\delta t$  varies with values ranging from 0.7 s up  
140 to 2.1 s. As for the eastern cluster, there is evidence for a contribution from LMM-  
141 anisotropy by taking  $\Delta SI$  into account, with values mostly  $> 0.4$  (Fig. DR10). Most non-  
142 discrepant pairs show clear nulls for both phases. A considerable amount of the  
143 corresponding pierce points is located close to or within the slow- $v_s$  anomaly beneath  
144 Iceland.

#### 145 **Nature of Anisotropy Below Siberia**

146 Below Siberia several global tomography models (including GyPSuM) agree in  
147 terms of relatively fast  $v_s$  (Shephard et al., 2017, Fig. DR12). This anomaly was  
148 interpreted as a remnant of paleosubducted slab material that is reaching down to the  
149 CMB (Van der Voo et al., 1999). This hypothesis is supported by previous (source- and  
150 receiver-side corrected) S-ScS splitting that revealed a dipping symmetry axis for the  
151 anisotropic fabric in a neighboring area (Wookey and Kendall, 2008). Furthermore, in a  
152 common geographical reference frame, the estimated orientation for  $\phi$  is similar to ours  
153 for a nearly east-west raypath (Fig. DR10). From geodynamic modeling it has been  
154 shown that sinking slab material can imprint strong strain-induced anisotropy at the base  
155 of the lower mantle (e.g., McNamara et al., 2002). Such a scenario is mainly controlled  
156 by the lattice-preferred orientation (LPO) of lower-mantle minerals like post-perovskite

157 (e.g., Merkel et al., 2007). Therefore, we infer that our discrepant SKS-SKKS  
158 observations indicate a widespread, so far unsampled region of coherent LPO-induced  
159 anisotropy in  $D''$ , caused by downwelling slab material that impinges on the CMB  
160 beneath Siberia (Fig. 4).

161 However, so far we cannot fully constrain the geometry of the anisotropic region due to  
162 limited ray coverage (except for events from the South Pacific area) and the observed  $\phi$ -  
163  $\delta t$  variations at most of our stations (Fig. DR2). Moreover, it remains unclear whether a  
164 change in the geometry or the mechanism of anisotropy is responsible for the significant  
165 difference in  $\phi$  between the split SKS and SKKS phases. Nevertheless, based on  
166 significant  $\Delta SI$  (Fig. DR10), we can demonstrate that a component of LMM-anisotropy  
167 contributes to the overall splitting signal.

#### 168 **Anisotropic Source Beneath the Atlantic**

169 Different global tomography models (including GyPSuM) consistently have  
170 anomalously low  $v_S$  and strong lateral velocity gradients from fast to slow seismic  
171 velocities along the northern edges of the African LLSVP beneath the Atlantic (Lekic et  
172 al., 2012, Fig. DR13). Beyond that, for some models also a potential connection between  
173 the African LLSVP and a 250-650 km-wide region of heavily reduced  $v_S$  ( $\sim -6\%$  to  $-10\%$ ,  
174 Fig. DR10) in  $D''$  below Iceland is detectable (e.g., He et al., 2015) which is located in  
175 the so far poorly sampled area of our 19 split SKKS observations up to  $\sim 50^\circ N$  (Fig. 3).  
176 These splitting observations are in good agreement with previous studies, suggesting  
177 strong and complex anisotropy along the edges of LLSVPs and meso-scale structures of  
178 similar character (e.g., Long and Lynner, 2015; Deng et al., 2017). In general, this  
179 anisotropy is assumed to be induced by complex mantle flow toward the boundaries of



180 the low- $v_s$  zones (e.g., Cottaar and Romanowicz, 2013). The absence of splitting within  
181 this zones, however, may indicate vertical mantle flow that feeds the upwelling hot  
182 mantle plume beneath Iceland (Fig. 4, He et al., 2015). Taking into account the overall  
183 splitting pattern at our long-running permanent stations (Fig. DR2), for most SKS phases  
184 from South American earthquakes we received clear nulls indicating no contributions  
185 from upper mantle anisotropy for these raypaths. In contrast, the SKKS phases of the  
186 same events exhibit consistent splitting with nearly the same orientation for  $\phi$ . Such a  
187 scenario allows us to suppose that the orientation of  $\phi$  (measured at the stations), mirrors  
188 the true direction of the anisotropy fast axis in the LMM without further influence from  
189 the upper mantle. Therefore our striking observations of mainly  $\Delta SI > 0.4$  in this area  
190 (Fig. DR10) support the idea that anisotropy is also located along the edges of the  
191 northern extensions of the African LLSVP towards the low- $v_s$  anomaly beneath Iceland.

## 192 CONCLUSIONS

193 Benefiting from a dense and large-aperture recording network in Scandinavia, we  
194 are able to explore two widespread areas on the fragmentary global map of LMM-  
195 anisotropy beneath the Atlantic and northwestern Siberia. While previous studies  
196 sampled several smaller partly overlapping patches of the LMM, with our observations of  
197 clearly discrepant SKS-SKKS splitting pairs we can draw a more complete picture of the  
198 whole area (Fig. DR14) although the geometry and mechanism of the anisotropic  $D''$   
199 fabrics cannot be fully derived from our results alone. Nevertheless, this demonstrates  
200 that the ongoing deployment of dense and large-aperture seismic networks not only helps  
201 to understand the anisotropic structure directly beneath a station itself but can also reveal

202 valuable and poorly needed information about extensive and dynamically active regions  
203 in  $D''$  relatively far away from the receiver.

#### 204 **ACKNOWLEDGMENTS**

205 This work has received funding from DFG (Deutsche Forschungsgemeinschaft)  
206 via LITHOS-CAPP (RI1133/11–1 and –2). Seismic data were obtained from the data  
207 centers GEOFON, Orfeus, IRIS and SEIS-UK as well as Univ. of Helsinki and the  
208 Swedish National Seismic Network (SNSN). Devices for the German contribution to  
209 ScanArray were provided by the GFZ GIPP instrument pool. Maps were prepared using  
210 GMT (Wessel et al., 2013). Abundant helpful comments on the manuscript by T.  
211 Hertweck and three anonymous reviewers are acknowledged.

#### 212 **REFERENCES CITED**

- 213 Bowman, J., and Ando, M., 1987, Shear-wave splitting in the upper-mantle wedge above  
214 the Tonga subduction zone: *Geophysical Journal of the Royal Astronomical Society*,  
215 v. 88, p. 25–41, <https://doi.org/10.1111/j.1365-246X.1987.tb01367.x>.
- 216 Chevrot, S., 2000, Multichannel analysis of shear wave splitting: *Journal of Geophysical*  
217 *Research*, v. 105, p. 21,579–21,590, <https://doi.org/10.1029/2000JB900199>.
- 218 Cottaar, S., and Romanowicz, B., 2013, Observations of changing anisotropy across the  
219 southern margin of the African LLSVP: *Geophysical Journal International*, v. 195,  
220 p. 1184–1195, <https://doi.org/10.1093/gji/ggt285>.
- 221 Crotwell, H.P., Owens, T.J., and Ritsema, J., 1999, The TauP toolkit: Flexible seismic  
222 travel-time and ray-path utilities: *Seismological Research Letters*, v. 70, p. 154–160,  
223 <https://doi.org/10.1785/gssrl.70.2.154>.

- 224 Deng, J., Long, M.D., Creasy, N., Wagner, L., Beck, S., Zandt, G., Tavera, H., and  
225 Minaya, E., 2017, Lowermost mantle anisotropy near the eastern edge of the Pacific  
226 LLSVP: Constraints from SKS-SKKS splitting intensity measurements: *Geophysical*  
227 *Journal International*, v. 210, p. 774–786, <https://doi.org/10.1093/gji/ggx190>.
- 228 Favier, N., and Chevrot, S., 2003, Sensitivity kernels for shear wave splitting in  
229 transverse isotropic media: *Geophysical Journal International*, v. 153, p. 213–228,  
230 <https://doi.org/10.1046/j.1365-246X.2003.01894.x>.
- 231 Grund, M., 2017, StackSplit - a plugin for multi-event shear wave splitting analyses in  
232 SplitLab: *Computers & Geosciences*, v. 105, p. 43–50,  
233 <https://doi.org/10.1016/j.cageo.2017.04.015>.
- 234 Grund, M., Mauerberger, A., Ritter, J.R.R., and Tilmann, F., 2017, Broadband  
235 Recordings for LITHOS-CAPP: LITHOspheric Structure of Caledonian, Archaean  
236 and Proterozoic Provinces Sep. 2014 - Oct. 2016, Sweden and Finland, STR-Data  
237 17/02, GIPP Experiment and Data Archive, Potsdam: GFZ German Research Centre  
238 for Geosciences, <https://doi.org/10.2312/GFZ.b103-17029>.
- 239 He, Y., Wen, L., Capdeville, Y., and Zhao, L., 2015, Seismic evidence for an Iceland  
240 thermo-chemical plume in the Earth's lowermost mantle: *Earth and Planetary*  
241 *Science Letters*, v. 417, p. 19–27, <https://doi.org/10.1016/j.epsl.2015.02.028>.
- 242 Lekic, V., Cottaar, S., Dziewonski, A., and Romanowicz, B., 2012, Cluster analysis of  
243 global lower mantle tomography: A new class of structure and implications for  
244 chemical heterogeneity: *Earth and Planetary Science Letters*, v. 357–358, p. 68–77,  
245 <https://doi.org/10.1016/j.epsl.2012.09.014>.

- 246 Lin, Y.-P., Zhao, L., and Hung, S.-H., 2014, Full-wave effects on shear wave splitting:  
247 Geophysical Research Letters, v. 41, p. 799–804,  
248 <https://doi.org/10.1002/2013GL058742>.
- 249 Long, M.D., 2009, Complex anisotropy in D'' beneath the eastern Pacific from SKS-  
250 SKKS splitting discrepancies: Earth and Planetary Science Letters, v. 283, p. 181–  
251 189, <https://doi.org/10.1016/j.epsl.2009.04.019>.
- 252 Long, M.D., and Lynner, C., 2015, Seismic anisotropy in the lowermost mantle near the  
253 Perm Anomaly: Geophysical Research Letters, v. 42, p. 7073–7080,  
254 <https://doi.org/10.1002/2015GL065506>.
- 255 Lynner, C., and Long, M.D., 2014, Lowermost mantle anisotropy and deformation along  
256 the boundary of the African LLSVP: Geophysical Research Letters, v. 41, p. 3447–  
257 3454, doi:<https://doi.org/10.1002/2014GL059875>.
- 258 McNamara, A.K., van Keken, P.E., and Karato, S.-I., 2002, Development of anisotropic  
259 structure in the Earth's lower mantle by solid-state convection: Nature, v. 416,  
260 p. 310–314, <https://doi.org/10.1038/416310a>.
- 261 Meade, C., Silver, P.G., and Kaneshima, S., 1995, Laboratory and seismological  
262 observations of lower mantle isotropy: Geophysical Research Letters, v. 22, p. 1293–  
263 1296, <https://doi.org/10.1029/95GL01091>.
- 264 Merkel, S., McNamara, A.K., Kubo, A., Speziale, S., Miyagi, L., Meng, Y., Duffy, T.S.,  
265 and Wenk, H.-R., 2007, Deformation of (Mg,Fe)SiO<sub>3</sub> post-perovskite and D''  
266 anisotropy: Science, v. 316, p. 1729–1732, <https://doi.org/10.1126/science.1140609>.

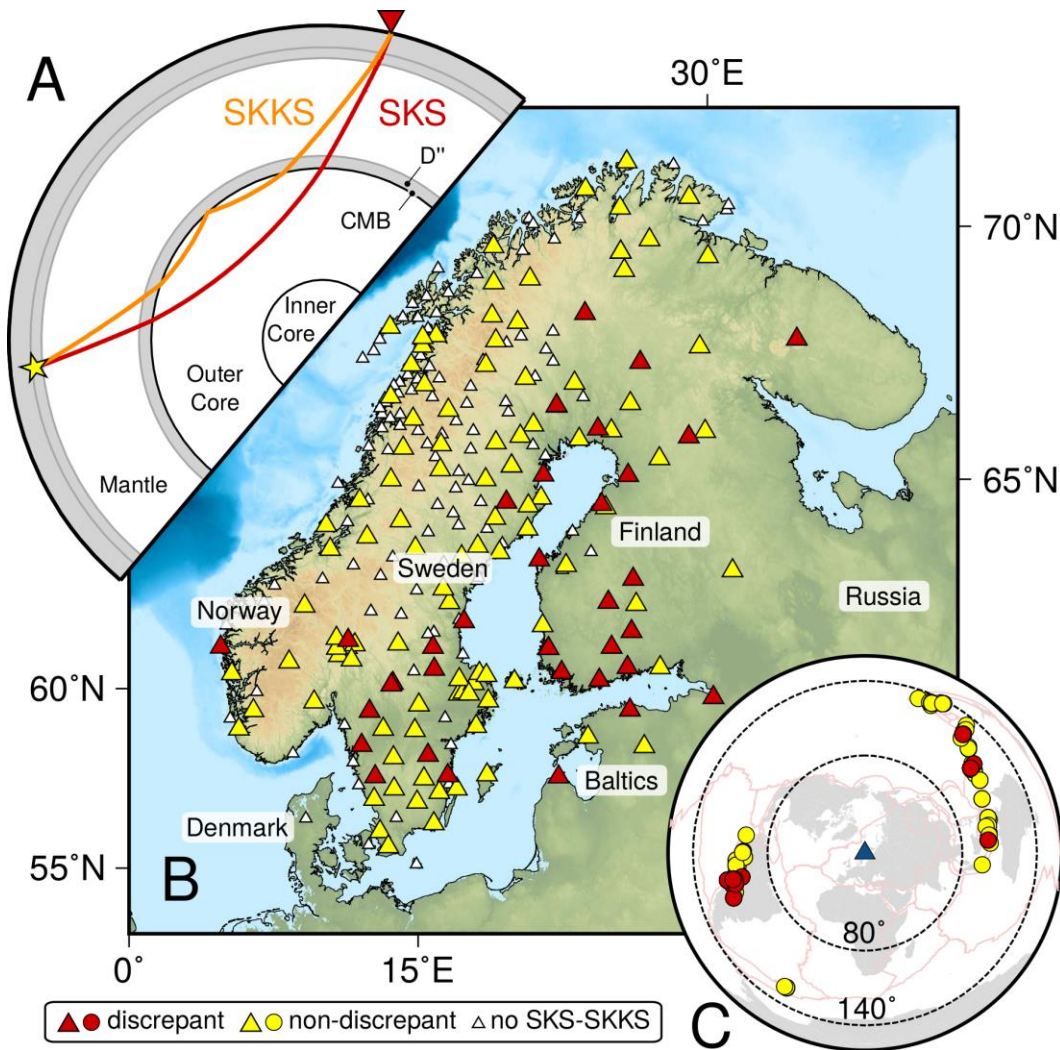
- 267 Niu, F., and Perez, A.M., 2004, Seismic anisotropy in the lower mantle: A comparison of  
268 waveform splitting of SKS and SKKS: *Geophysical Research Letters*, v. 31,  
269 p. L24612, <https://doi.org/10.1029/2004GL021196>.
- 270 Shephard, G.E., Matthews, K.J., Hosseini, K., and Domeier, M., 2017, On the  
271 consistency of seismically imaged lower mantle slabs: *Scientific Reports*, v. 7,  
272 p. 10976, <https://doi.org/10.1038/s41598-017-11039-w>.
- 273 Silver, P.G., and Chan, W.W., 1991, Shear wave splitting and subcontinental mantle  
274 deformation: *Journal of Geophysical Research*, v. 96, p. 16429–16454,  
275 <https://doi.org/10.1029/91JB00899>.
- 276 Simmons, N.A., Forte, A., Boschi, L., and Grand, S., 2010, GyPSuM: A joint  
277 tomographic model of mantle density and seismic wave speeds: *Geophysical*  
278 *Research Letters*, v. 115, B12310, <https://doi.org/10.1029/2010JB007631>.
- 279 Thybo, H., Balling, N., Maupin, V., Ritter, J., and Tilmann, F., 2012, ScanArray Core  
280 (1G 2012–2017): The ScanArray consortium, Other/Seismic Network,  
281 <http://doi.org/10.14470/6T569239>.
- 282 Van der Voo, R., Spakman, W., and Bijwaard, H., 1999, Mesozoic subducted slabs under  
283 Siberia: *Nature*, v. 397, p. 246–249, <https://doi.org/10.1038/16686>.
- 284 Walsh, E., Arnold, R., and Savage, M.K., 2013, Silver and Chan revisited: *Journal of*  
285 *Geophysical Research*, v. 118, p. 5500–5515.
- 286 Wessel, P., Smith, W.H.F., Scharroo, R., Luis, J., and Wobbe, F., 2013, Generic Mapping  
287 Tools: Improved version released: *Eos Transactions, American Geophysical Union*,  
288 v. 94, p. 409–420.

289 Wookey, J., and Kendall, J.-M., 2008, Constraints on lowermost mantle mineralogy and  
290 fabric beneath Siberia from seismic anisotropy: Earth and Planetary Science Letters,  
291 v. 275, p. 32–42, <https://doi.org/10.1016/j.epsl.2008.07.049>.

292 Wüstefeld, A., Bokelmann, G., Zaroli, C., and Barruol, G., 2008, SplitLab: A shear-wave  
293 splitting environment in Matlab: Computers & Geosciences, v. 34, p. 515–528,  
294 <https://doi.org/10.1016/j.cageo.2007.08.002>.

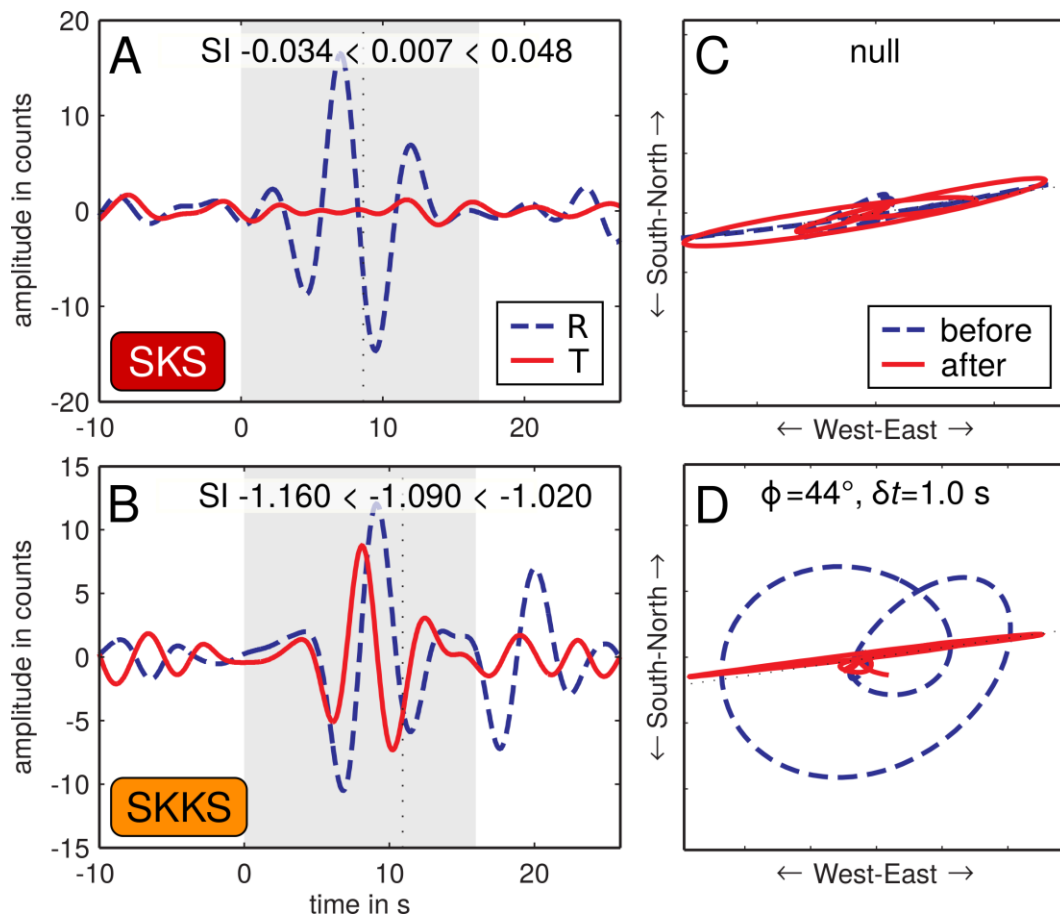
295

296 **FIGURES AND CAPTIONS**



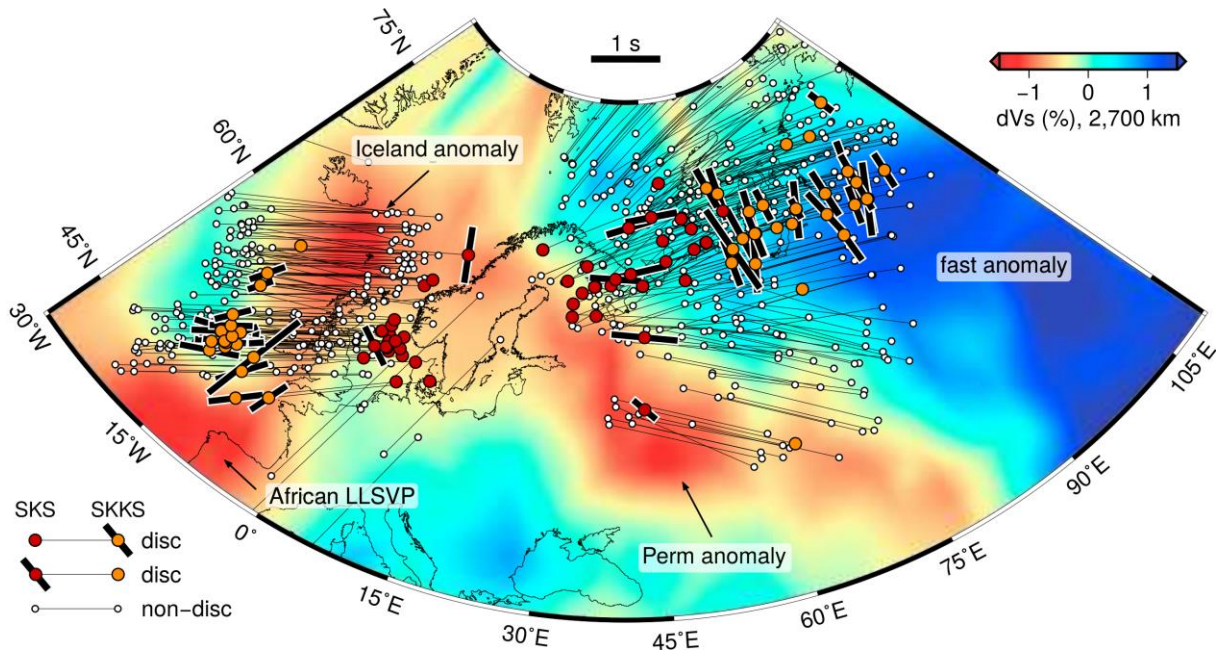
297

298 Figure 1. A: SKS-SKKS raypaths from hypocenter (star) to receiver (500 km depth,  $\Delta$   
299  $\sim 100^\circ$ ). B: Seismic stations used in this study (triangles). Color fill represents the  
300 observation of SKS-SKKS waveforms, with red for at least one discrepant pair and  
301 yellow for only non-discrepant recordings. White triangles display sites at which no SKS-  
302 SKKS pairs were observed. C: Distribution of earthquakes that yielded at least one  
303 discrepant (red) or non-discrepant (yellow) SKS-SKKS pair.  
304



305  
306 Figure 2. A and B: Original (uncorrected) radial (R, blue dashed) and transverse (T, solid  
307 red) component seismograms at station PVF for SKS (top) and SKKS (bottom) of the  
308 same event at 25/07/2016. At the top the splitting intensity (SI) value along with its

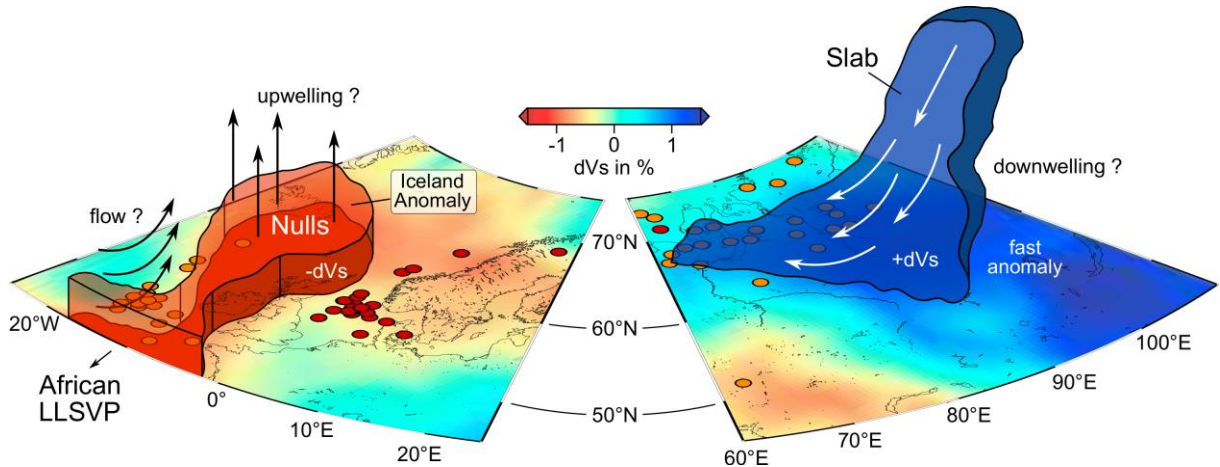
309 uncertainty (95% confidence interval) is shown. C and D: Particle motions before (blue  
310 dashed) and after (solid red) correcting the splitting using the Silver and Chan (1991)  
311 method. Splitting parameters  $\phi$  and  $\delta t$  or null are indicated at the top of each panel.  
312



313  
314 Figure 3. D'' pierce points of SKS-SKKS pairs calculated with the tauP toolkit based on  
315 the iasp91 earth model (Crotwell et al., 1999) atop the GyPSuM global vs tomography  
316 model at 2,700 km depth (Simmons et al., 2010). Discrepant pairs are marked with red  
317 (SKS) and orange (SKKS) dots, the split phase is indicated with a black bar oriented in  
318 the direction of  $\phi$  and scaled by  $\delta t$  (as observed at the station). Related pierce points are  
319 connected by thin black lines. White dots indicate non-discrepant pairs.

320  
321





322

323 Figure 4. Interpretation of our findings based on two of the most plausible sources of  $D''$   
324 anisotropy. Beneath the Atlantic, nearly horizontal mantle flow potentially induces  
325 anisotropy along the northern extensions of the African Large Low Shear Velocity  
326 Province (LLSVP) toward the Iceland Anomaly. Absence of splitting (null) is observed  
327 for the majority of measurements that correspond to pierce points located within the  
328 Iceland Anomaly and potentially indicates vertical flow. Beneath Siberia downwelling  
329 (colder than average) material of a subducted slab imprints anisotropy in a widespread  
330 area atop the core-mantle boundary.

331

332 <sup>1</sup>GSA Data Repository item **2019049**, Table DR1 (individual splitting measurements) and  
333 Figures DR2-DR14 (stereoplots, examples of SKS-SKKS and sSKS splitting, Fresnel  
334 zone estimates, event statistics, two record sections, map of split-split pairs, map of  $\Delta SI$ ,  
335 geological units, model agreement for fast and slow  $v_s$ , overview LMM studies), is  
336 available online at <http://www.geosociety.org/datarepository/2019/>, or on request from  
337 [editing@geosociety.org](mailto:editing@geosociety.org).